Available online at www.sciencedirect.com
SCIENCE DIRECT®
Journal of Sound and Vibration 278 (2004) 657–684
JOURNAL OF SOUND AND VIBRATION
www.elsevier.com/locate/jsvi

Free vibration analysis of plates by using a four-node finite element formulated with assumed natural transverse shear strain

S.J. Lee*

Integrated Safety Assessment Division, Korea Atomic Energy Research Institute, P.O. Box 105, Yuseong, Daejeon 306-600, South Korea

Received 5 November 2002; accepted 16 October 2003

Abstract

A study on the free vibration analysis of plates is described in this paper. In order to investigate vibrational characteristics of plates, a four-node plate element is developed by using the assumed natural strains on the basis of Reissner–Mindlin (RM) assumptions which allows us to consider the shear deformation and rotatory inertia effect. All terms related to the plate finite element formulation are consistently defined in the natural domain. Assumed natural strains are derived to alleviate the locking phenomena inherited in the RM plate elements. In particular, the explicit expression of assumed natural transverse shear strain is described in this paper. The natural constitutive equation is used in conjunction with the natural strain terms. Several numerical examples are carried out and their results are then compared with the existing reference solutions.

1. Introduction

For years, there has been a large amount of research work on the free vibration analysis of plate structures. In the early days, analytical methods were widely adopted but soon the finite element (FE) technology became the most popular approach of assessing vibrational characteristics of the plates in engineering practices.

The extensive review on plate vibration can be found in the literature provided by Leissa [1–4] and more recently, Liew [5] provided some review on thick plate vibration problems. For thick plate problems, the Reissner–Mindlin (RM) assumptions [6] have been generally adopted in the

*Current address: Department of Architectural Engineering, Gyeongsang National University, 900 Gazwa-dong, Jinju City 660-701, South Korea.

E-mail address: sjlee@kaeri.re.kr (S.J. Lee).

0022-460X/$ - see front matter
doi:10.1016/j.jsv.2003.10.018

development of plate elements. It has been shown that the accuracy of the frequency is improved by the shear deformation and rotatory inertia effects included in the stiffness and mass matrices, respectively. However, it is found that there are serious defects such as the locking phenomena in the RM plate element.

As an early remedy of the locking phenomena inherited in the thick plate element based on RM assumptions, the so-called reduced integration [7,8] was used in the transverse shear energy term. But the plate elements with the reduced integration suffered from the mechanism and later other methods, such as assumed strain methods [9] and stabilization method [10], have been proposed by many researchers. The assumed strain methods have been successfully used in stress FE analysis. But contrarily there is little investigation on the performance of the assumed strained FEs [11–14], in particular lower order plate element, in free vibration analysis.

In this paper, therefore, a bilinear plate FE formulation based on the natural domain is provided with emphasis on the terms related to the stiffness and mass matrices. Then, a set of benchmarks are presented to show the applicability of the present plate element to various types of plates under free vibration conditions. Note that the Gauss integration rule is adopted to evaluate the consistent mass matrix and subspace iteration method [15] is employed in the calculation of the lowest eigenvalues of plates. It should be noted that the lumped mass matrix derived by the HRZ method [16] is also used in analysis to produce FE reference solutions for future study.

2. Reissner–Mindlin assumptions

The following basic assumptions of RM plate theory are employed throughout this study:

- The normal to the mid-surface of plate remains straight after deformation but not necessarily normal to the deformed mid-surface.
- The normal transverse stress is negligible as in Kirchhoff–Love theory.
- The displacements are small compared to the plate thickness.

Numerical integration through the thickness direction is facilitated by the first assumption and the constitutive equation is simplified by the second assumption.

From the first assumption of the RM theory, the displacement field of plate element will have only C^o continuity and it can be illustrated as shown in Fig. 1.

3. Assumed strain field

In the plate formulation, standard definition of natural strains [14] can be used. However, the RM plate element produces the shear locking phenomena and the assumed strain formulation is therefore employed in this study. There are two main steps in order to derive the assumed strain field:

- the calculation of the positions of the sampling points for the assumed strain field,
- the interpolation of the assumed strains using standard strains calculated at sampling points.

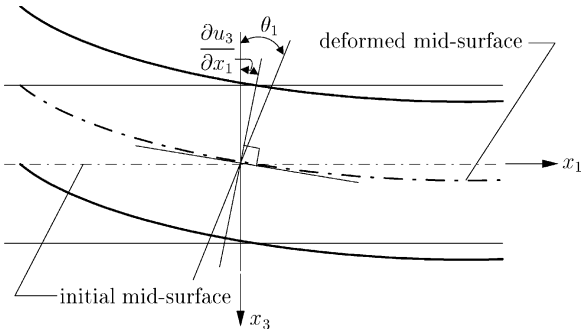

Fig. 1. Reissner–Mindlin assumptions.

Here, the procedure calculating the sampling points and the derivation of assumed natural strains for a bilinear plate element are presented.

3.1. The position of sampling points

The positions of sampling points are the locations [13,14] where the locking does not exist. It is extremely important to find reasonable sampling points since the assumed strains will be interpolated using the strains calculated at sampling points. In this section, the procedure of calculation of sampling points is described for four-node plate bending element which normally exhibits transverse shear lockings with the standard displacement formulation. RM assumptions with the plate bending situation is used to determine the positions of sampling points for transverse shear strains.

With RM assumptions, the displacement components due to bending at point (x_1, x_2, x_3) can be expressed in the global co-ordinate system as (see Fig. 2)

$$\begin{aligned} u_i &= x_3\theta_i(x_1, x_2) \quad (i = 1, 2), \\ u_3 &= u_3(x_1, x_2), \end{aligned} \tag{1}$$

where u_1 are u_2 are the in-plane displacement components, u_3 is the transverse deflection, θ_1 is the normal rotation in x_1–x_3 plane, and θ_2 is the normal rotation in x_2–x_3 plane.

The transverse shear strain components in the global co-ordinate system are

$$\varepsilon_{3i} = \frac{\partial u_i}{\partial x_3} + \frac{\partial u_3}{\partial x_i} \quad (i = 1, 2). \tag{2}$$

The above equation can be rewritten in view of Eq. (1)

$$\varepsilon_{3i} = \theta_i + \frac{\partial u_3}{\partial x_i} \quad (i = 1, 2). \tag{3}$$

At this stage, natural strain components are introduced to treat this problem efficiently. The natural transverse shear strain can be written by using the tensor transformation.

$$\tilde{\varepsilon}_{3\alpha} = \frac{\partial x_i}{\partial \xi_\alpha}\varepsilon_{3i} \quad (\alpha = 1, 2; i = 1, 2 \text{ summed}). \tag{4}$$

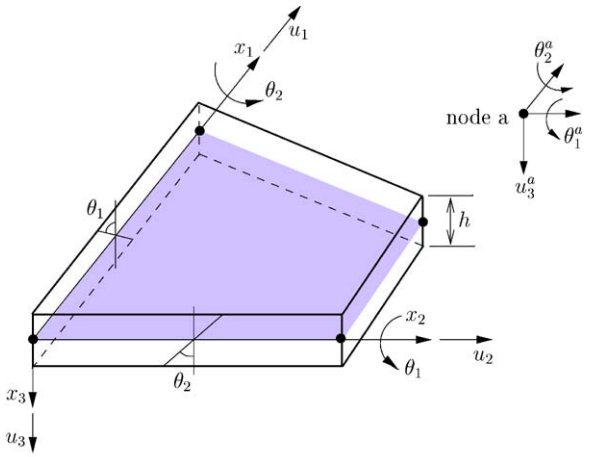

Fig. 2. Plate bending element sign convention.

Substituting Eq. (3) into Eq. (4) yields

$$\tilde{\varepsilon}_{3\alpha} = \frac{\partial x_i}{\partial \xi_\alpha}\theta_i + \frac{\partial u_3}{\partial \xi_\alpha} \quad (\alpha = 1,2; i = 1,2 \text{ summed})$$
$$= \tilde{\theta}_\alpha + \frac{\partial u_3}{\partial \xi_\alpha} \quad (\alpha = 1,2). \tag{5}$$

Note that the strain components ε_{3i} in the global co-ordinate system can be obtained by inversion of Eq. (4) as

$$\varepsilon_{3i} = \frac{\partial \xi_\alpha}{\partial x_i}\tilde{\varepsilon}_{3\alpha} \quad (\alpha = 1,2 \text{ summed}; i = 1,2). \tag{6}$$

Physically, transverse shear strains will vanish if the thickness–span ratio of the plate is extremely small:

$$\tilde{\varepsilon}_{3\alpha} = 0 \quad (\alpha = 1,2), \tag{7}$$

or

$$\tilde{\theta}_\alpha = -\frac{\partial u_3}{\partial \xi_\alpha} \quad (\alpha = 1,2). \tag{8}$$

It is now clear that the polynomial of term $\tilde{\theta}_\alpha$ of Eq. (8) is one order higher than that of the term $\partial u_3/\partial \xi_\alpha$. Therefore, it is not possible to achieve Eq. (7). In order to solve the inconsistency of the order of two terms, we may have two solutions as follows

- The coefficients of higher order term in $\tilde{\theta}_\alpha$ should be enforced to be zero.
- All terms presented in the expression of $\tilde{\theta}_\alpha$ may have their counterpart in the expression of $\partial u_3/\partial \xi_\alpha$.

In this study, the second solution is adopted and new assumed displacement field $\tilde{u}_3$ is introduced. Therefore, the polynomial terms of $\partial u_3/\partial\xi_\alpha$ can include all terms of the $\tilde{\theta}_\alpha$. The assumed biquadratic displacement field $\tilde{u}_3$ can be written as

$$\tilde{u}_3 = \sum_{p,q=0}^{2} c_{pq}(\xi_1)^p(\xi_2)^q. \tag{9}$$

Since the procedure for calculating the sampling point is similar to each other, the calculation of the sampling points for the term $\tilde{\varepsilon}_{31}$ of four-node element is only presented here. For four-node Lagrangian element, the rotation and deflection fields $\theta_i (i = 1, 2)$ and u_3 are

$$\theta_i = \sum_{a=1}^{4} N_a(\xi_1, \xi_2)\theta_i^a \quad (i = 1, 2),$$

$$u_3 = \sum_{a=1}^{4} N_a(\xi_1, \xi_2)u_3^a, \tag{10}$$

where $N_a(\xi_1, \xi_2)$ is the linear Lagrange shape function associated with node a such as

$$N_a(\xi_1, \xi_2) = \tfrac{1}{4}(1 + \xi_1^a\xi_1)(1 + \xi_2^a\xi_2), \tag{11}$$

where ξ_1^a, ξ_2^a denote the position of nodal point a according to natural co-ordinate system.

Let the bilinear approximation of deflection be

$$u_3 = \sum_{a=1}^{4} N_a\tilde{u}_3^a, \tag{12}$$

where $\tilde{u}_3^a$ is the nodal displacement value at node a calculated using assumed displacement field of Eq. (9) and Eq. (12) can be rewritten in the explicit form as

$$u_3 = (c_{00} + c_{20} + c_{02} + c_{22}) + (c_{10} + c_{12})\xi_1 + (c_{01} + c_{21})\xi_2. \tag{13}$$

Enforcing the equality of derivatives of u_3 and $\tilde{u}_3$ with respect to ξ_1

$$\frac{\partial u_3}{\partial\xi_1} = \frac{\partial\widetilde{u_3}}{\partial\xi_1}, \tag{14}$$

yields

$$2\xi_1(c_{20} + c_{21}\xi_2 + c_{22}(\xi_2)^2) + c_{12}((\xi_2)^2 - 1) = 0. \tag{15}$$

For arbitrary values of c_{20}, c_{21}, c_{22} and c_{12}, the following solutions to Eq. (15) can be obtained:

$$\xi_1 = 0, \ \ \xi_2 = 1 \quad \text{and} \quad \xi_1 = 0, \ \ \xi_2 = -1. \tag{16}$$

Another set of the sampling points for $\tilde{\varepsilon}_{32}$ can be calculated by the same procedure used for $\tilde{\varepsilon}_{31}$ and those are

$$\xi_1 = 1, \ \ \xi_2 = 0 \quad \text{and} \quad \xi_1 = -1, \ \ \xi_2 = 0. \tag{17}$$

The position of the sampling points for $\tilde{\varepsilon}_{31}$ and $\tilde{\varepsilon}_{32}$ is illustrated in Fig. 3.

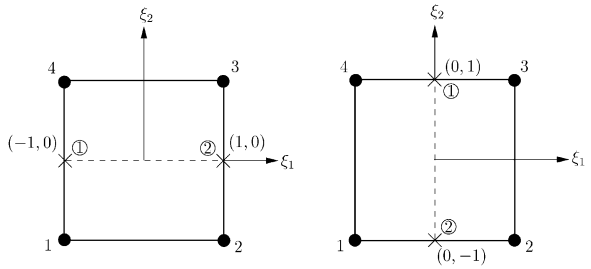

Fig. 3. The position of sampling point: (left) $\tilde{\varepsilon}_{31}$ and (right) $\tilde{\varepsilon}_{32}$.

3.2. Assumed natural strains

The interpolation functions used in the formulation of assumed strains are based on Lagrangian polynomial and the position of sampling points in the previous section. Therefore, the assumed natural strains are defined as follows:

$$\tilde{\varepsilon}_{13}^{(a)} = \sum_{\delta=1}^{2} P_\delta(\xi_2)\tilde{\varepsilon}_{13}^{\delta}, \quad \tilde{\varepsilon}_{23}^{(a)} = \sum_{\delta=1}^{2} Q_\delta(\xi_1)\tilde{\varepsilon}_{23}^{\delta}, \tag{18}$$

in which δ denotes the position of the sampling point as shown in Fig. 3 and the interpolation functions P and Q are

$$\begin{aligned} P_1(\xi) &= \tfrac{1}{2}(1-\xi), \quad P_2(\xi) = \tfrac{1}{2}(1+\xi), \\ Q_1(\xi) &= \tfrac{1}{2}(1+\xi), \quad Q_2(\xi) = \tfrac{1}{2}(1-\xi). \end{aligned} \tag{19}$$

Finally, we can write the explicit form of assumed strains for a four-node RM plate element in the following form:

$$\begin{aligned} \tilde{\varepsilon}_{31}^{(a)} =& \tfrac{1}{4}\xi_1^a(1+\xi_2^a\xi_2)u_3^a \\ &+ \tfrac{1}{4}[\alpha_1(1+\xi_2^a\xi_2)+\beta_1(\xi_2^a+\xi_2)]\theta_1^a \\ &+ \tfrac{1}{4}[\alpha_2(1+\xi_2^a\xi_2)+\beta_2(\xi_2^a+\xi_2)]\theta_2^a, \end{aligned} \tag{20}$$

$$\begin{aligned} \tilde{\varepsilon}_{32}^{(a)} =& \tfrac{1}{4}\xi_2^a(1+\xi_1^a\xi_1)u_3^a \\ &+ \tfrac{1}{4}[\gamma_1(1+\xi_1^a\xi_1)+\beta_1(\xi_1^a+\xi_1)]\theta_1^a \\ &+ \tfrac{1}{4}[\gamma_2(1+\xi_1^a\xi_1)+\beta_2(\xi_1^a+\xi_1)]\theta_2^a, \end{aligned} \tag{21}$$

where the parameters $\alpha_1, \beta_1, \gamma_1, \alpha_2, \beta_2, \gamma_2$ are

$$\begin{aligned} \alpha_1 &= \tfrac{1}{4}(-x_1^1 + x_1^2 + x_1^3 - x_1^4), \\ \beta_1 &= \tfrac{1}{4}(x_1^1 - x_1^2 + x_1^3 - x_1^4), \\ \gamma_1 &= \tfrac{1}{4}(-x_1^1 - x_1^2 + x_1^3 + x_1^4), \\ \alpha_2 &= \tfrac{1}{4}(-x_2^1 + x_2^2 + x_2^3 - x_2^4), \\ \beta_2 &= \tfrac{1}{4}(x_2^1 - x_2^2 + x_2^3 - x_2^4), \\ \gamma_2 &= \tfrac{1}{4}(-x_2^1 - x_2^2 + x_2^3 + x_2^4), \end{aligned} \tag{22}$$

where x_i^a denotes the ith component of the position vector $\mathbf{x}$ at node a in global co-ordinate system. The assumed natural transverse shear strains of Eqs. (20) and (21) are used instead of the standard transverse shear strain terms in this study.

4. Constitutive equation

The stress tensor for elastically isotropic materials can be written as

$$\sigma_{ij} = D_{ijkl}\varepsilon_{kl} = [\lambda\delta_{ij}\delta_{kl} + \mu(\delta_{ik}\delta_{jl} + \delta_{il}\delta_{jk})]\varepsilon_{kl}, \tag{23}$$

where σ_{ij} is the Cauchy stress, D_{ijkl} is a fourth order isotropic material tensor and ε_{kl} is the small strains. λ and μ are the Lamé constants and δ_{ij} is the Kronecker delta. An isotropic material is not direction dependent. However, a scaling factor has to be introduced when elastic constants are formed in the natural domain. The natural stress tensor can be written as follows:

$$\tilde{\sigma}_{\alpha\beta} = \tilde{D}_{\alpha\beta\gamma\delta}\tilde{\varepsilon}_{\gamma\delta} = \tilde{J}[\lambda g_{\alpha\beta}g_{\gamma\delta} + \mu(g_{\alpha\gamma}g_{\beta\delta} + g_{\alpha\delta}g_{\beta\gamma})]\tilde{\varepsilon}_{\gamma\delta}, \tag{24}$$

where the natural constitutive tensor is obtained from

$$\tilde{D}_{\alpha\beta\gamma\delta} = \tilde{J}\frac{\partial\xi_\alpha}{\partial x_i}\frac{\partial\xi_\beta}{\partial x_j}\frac{\partial\xi_\gamma}{\partial x_k}\frac{\partial\xi_\delta}{\partial x_l}D_{ijkl}, \tag{25}$$

and $\tilde{J} = \det[\partial x_i/\partial\xi_\alpha]$ and $g_{\alpha\beta} = \partial\xi_\alpha/\partial x_i\partial\xi_\beta/\partial x_i$.

The above equation can be reduced using the generalized plane stress condition $\tilde{\sigma}_3 = 0$ as follows:

$$\tilde{D}^*_{\alpha\beta\gamma\delta} = \bar{J}[\bar{\lambda}\bar{g}_{\alpha\beta}\bar{g}_{\gamma\delta} + \mu(\bar{g}_{\alpha\gamma}\bar{g}_{\beta\delta} + \bar{g}_{\alpha\delta}\bar{g}_{\beta\gamma})], \tag{26}$$

where $\bar{\lambda}$ is the reduced Lamé constant for the generalized plane stress–strain relationship, $\bar{J}$ and $\bar{g}_{\alpha\beta}$ are calculated using $\tilde{J}$ and $\tilde{g}_{\alpha\beta}$ at $\xi_3 = 0$.

Now the natural stresses can be rewritten in matrix form as

$$\begin{Bmatrix} \tilde{\boldsymbol{\sigma}}_p \\ \tilde{\boldsymbol{\sigma}}_s \end{Bmatrix} = \begin{bmatrix} \tilde{\mathbf{D}}^*_p & 0 \\ 0 & \tilde{\mathbf{D}}^*_s \end{bmatrix} \begin{Bmatrix} \tilde{\boldsymbol{\varepsilon}}_p \\ \tilde{\boldsymbol{\varepsilon}}_s \end{Bmatrix}, \tag{27}$$

where $\tilde{\boldsymbol{\sigma}}_p = [\tilde{\sigma}_{11}, \tilde{\sigma}_{22}, \tilde{\sigma}_{12}]^{\mathrm{T}}$ is the in-plane stress term and $\tilde{\boldsymbol{\sigma}}_s = [\tilde{\sigma}_{13}, \tilde{\sigma}_{23}]^{\mathrm{T}}$ is the transverse shear stress term and the natural in-plane and transverse shear rigidity matrices $\tilde{\mathbf{D}}^*_p, \tilde{\mathbf{D}}^*_s$ are

$$\tilde{\mathbf{D}}^*_p = \bar{J}\begin{bmatrix} \alpha\bar{g}_{11}^2 & \beta\bar{g}_{11}\bar{g}_{22} + 2\bar{g}_{12}^2 & \alpha\bar{g}_{11}\bar{g}_{12} \\ \beta\bar{g}_{11}\bar{g}_{22} + 2\bar{g}_{12}^2 & \alpha\bar{g}_{22}^2 & \alpha\bar{g}_{12}\bar{g}_{22} \\ \alpha\bar{g}_{11}\bar{g}_{12} & \alpha\bar{g}_{12}\bar{g}_{22} & \beta\bar{g}_{12}^2 + \mu(\bar{g}_{11}\bar{g}_{22} + \bar{g}_{12}^2) \end{bmatrix}, \tag{28}$$

$$\tilde{\mathbf{D}}^*_s = \bar{J}\begin{bmatrix} k_s\mu\bar{g}_{11}\bar{g}_{33} & k_s\mu\bar{g}_{12}\bar{g}_{33} \\ k_s\mu\bar{g}_{12}\bar{g}_{33} & k_s\mu\bar{g}_{22}\bar{g}_{33} \end{bmatrix}, \tag{29}$$

in which, the parameters α and β are

$$\alpha = \frac{4\mu(\lambda+\mu)}{\lambda+2\mu} = \frac{E}{1-\nu^2} \quad \text{and} \quad \beta = \frac{2\mu\lambda}{\lambda+2\mu} = \frac{\nu E}{1-\nu^2} \tag{30}$$

and k_s is the shear correction factor which is in general taken as 5/6 for an isotropic material and v is the Poisson ratio.

In the plate problem, the global co-ordinate x_3 coincides with the natural co-ordinate ξ_3 and therefore the term $\bar{g}_{33}$ is equal to 1 and the transverse shear rigidity matrix $\tilde{\mathbf{D}}_s^*$ can be finally written as

$$\tilde{\mathbf{D}}_s^* = \bar{J}\begin{bmatrix} k_s\mu\bar{g}_{11} & k_s\mu\bar{g}_{12} \\ k_s\mu\bar{g}_{12} & k_s\mu\bar{g}_{22} \end{bmatrix}. \tag{31}$$

After forming the natural co-ordinate-based stress–strain relationship, stress resultants constitutive model could be obtained by taking pre-integration of thickness direction. Finally, the stress resultants constitutive equation used in this study can be written as

$$\{\tilde{M}_1, \tilde{M}_2, \tilde{M}_{12}\} = \int_{\tilde{\ell}} \xi_3\{\tilde{\sigma}_{11}, \tilde{\sigma}_{22}, \tilde{\sigma}_{12}\}\,\mathrm{d}\xi_3,$$
$$\{\tilde{Q}_1, \tilde{Q}_2\} = \int_{\tilde{\ell}} \{\tilde{\sigma}_{13}, \tilde{\sigma}_{23}\}\,\mathrm{d}\xi_3 \tag{32}$$

and the above stress resultant relationship can be written in matrix form as

$$\begin{Bmatrix} \tilde{\mathbf{M}} \\ \tilde{\mathbf{Q}} \end{Bmatrix} = \begin{bmatrix} \tilde{\mathbf{D}}^* & 0 \\ 0 & \tilde{\mathbf{G}}^* \end{bmatrix} \begin{Bmatrix} \tilde{\boldsymbol{\kappa}} \\ \tilde{\boldsymbol{\varepsilon}}_s \end{Bmatrix}, \tag{33}$$

where the components of the rigidity matrix are

$$\tilde{\mathbf{D}}^* = \int_{\tilde{\ell}} \xi_3^2 \tilde{\mathbf{D}}_p^*\,\mathrm{d}\xi_3, \quad \tilde{\mathbf{G}}^* = \int_{\tilde{\ell}} k_s \tilde{\mathbf{D}}_s^*\,\mathrm{d}\xi_3 \tag{34}$$

in which $\tilde{\mathbf{D}}^*$ $(i,j = 1,3)$ and $\tilde{\mathbf{G}}^*$ $(i,j = 4,5)$ are respectively bending and transverse shear stiffness coefficients; k_s is the shear correction factor.

5. Mass matrix

In this section, the mass matrices for the plate elements are described. The consistent element mass matrix for four-node plate element can be written as

$$\mathbf{M}^{(e)} = \mathbf{M}_{ab}^{(e)} = \int_{\tilde{V}^{(e)}} (\mathbf{N}_a)^{\mathrm{T}} \tilde{\rho} \mathbf{N}_b \tilde{J}\,\mathrm{d}\tilde{V}, \tag{35}$$

where a, b are the number of element nodes and ρ is the density of the mass.

The mass matrix $\mathbf{M}_{ab}^{(e)}$ can be written as

$$\mathbf{M}_{ab}^{(e)} = \begin{bmatrix} \breve{m}_{ab} & 0 & 0 \\ 0 & \breve{m}_{ab} & 0 \\ 0 & 0 & \breve{m}_{ab} \end{bmatrix}, \tag{36}$$

where the translational mass $\bar{m}_{ab}$ and the rotational mass $\breve{m}_{ab}$ matrices linking to nodes a and b can be written as

$$\bar{m}_{ab} = \int_{\tilde{A}^{(e)}} \tilde{\rho}[N_a N_b h]\bar{J}\,\mathrm{d}\tilde{A}; \quad \breve{m}_{ab} = \int_{\tilde{A}^{(e)}} \tilde{\rho}[N_a N_b h^3/12]\bar{J}\,\mathrm{d}\tilde{A}. \tag{37}$$

The above consistent mass matrix can be reformulated into lumped mass matrix [16] which has only its diagonal components. The diagonal translational mass term $\bar{m}_{aa}$ and the diagonal rotatory inertia terms $\breve{m}_{aa}$ associated with the base vectors $\hat{e}_1^a$ and $\hat{e}_2^a$ of the global co-ordinate system at the node a can be written as

$$\bar{m}_{aa}^* = \int_{\tilde{V}^{(e)}} w_a \tilde{\rho}\tilde{J}\,\mathrm{d}\tilde{V}; \quad \breve{m}_{aa}^* = \int_{\tilde{V}^{(e)}} w_a \rho \xi_3^2 \tilde{J}\,\mathrm{d}\tilde{V}, \tag{38}$$

where ρ is the mass density and the multiplier w_a can be written as

$$w_a = \frac{\int_{\tilde{V}^{(e)}} \tilde{\rho} N_a N_a \tilde{J}\,\mathrm{d}\tilde{V}}{\sum_{k=1}^{n} \int_{\tilde{V}^{(e)}} \tilde{\rho} N_k N_k \tilde{J}\,\mathrm{d}\tilde{V}} \tag{39}$$

in which n is the number of node for each element.

Therefore, the lumped diagonal mass matrix at node a can be written in matrix form as

$$\mathbf{M}_{aa}^{(e)*} = \begin{bmatrix} \bar{m}_{aa}^* & 0 & 0 \\ 0 & \breve{m}_{aa}^* & 0 \\ 0 & 0 & \breve{m}_{aa}^* \end{bmatrix}. \tag{40}$$

Note that Gauss quadrature scheme is used to calculate both the consistent mass matrix and the lumped mass matrix.

6. Equilibrium equation

In the absence of external loads and damping effects, the dynamic equilibrium equation [14] based on the principle of virtual work (or more precisely virtual power) can be written as

$$\int_{\Omega} [\delta\boldsymbol{\varepsilon}_p^{\mathrm{T}} \mathbf{D}_p \boldsymbol{\varepsilon}_p + \delta\boldsymbol{\varepsilon}_s^{\mathrm{T}} \mathbf{D}_s \boldsymbol{\varepsilon}_s]\,\mathrm{d}\Omega + \int_{\Omega} [\delta\mathbf{u}]^{\mathrm{T}} \rho \ddot{\mathbf{u}}\,\mathrm{d}\Omega = 0. \tag{41}$$

For a discretized FE domain, the displacement field can be expressed in terms of the nodal displacements $\mathbf{u}^a$ and the global shape functions $\hat{\mathbf{N}}_a$ [17] which are constructed from local shape functions N_a and the acceleration can be also written in the same way

$$\mathbf{u} = \sum_{a=1}^{np} \hat{\mathbf{N}}_a(\xi_1, \xi_2)\mathbf{u}^a, \quad \ddot{\mathbf{u}} = \sum_{a=1}^{np} \hat{\mathbf{N}}_a(\xi_1, \xi_2)\ddot{\mathbf{u}}^a, \tag{42}$$

where np is the total number of the node in the discretized domain and the virtual terms associated with the displacement and acceleration are

$$\delta\mathbf{u} = \sum_{a=1}^{np} \hat{\mathbf{N}}_a(\xi_1, \xi_2)\delta\mathbf{u}^a, \quad \delta\ddot{\mathbf{u}} = \sum_{a=1}^{np} \hat{\mathbf{N}}_a(\xi_1, \xi_2)\delta\ddot{\mathbf{u}}^a. \tag{43}$$

The strain–displacement and virtual strain–displacement relationships can then be written as

$$\boldsymbol{\varepsilon} = \sum_{a=1}^{np} \hat{\mathbf{B}}^a \mathbf{u}^a, \quad \delta\boldsymbol{\varepsilon} = \sum_{a=1}^{np} \hat{\mathbf{B}}^a \delta\mathbf{u}^a, \tag{44}$$

where $\hat{\mathbf{B}}^a$ is the global strain–displacement matrix which are constructed from local strain–displacement matrix $\mathbf{B}^a$.

Substituting Eqs. (42)–(44) into Eq. (41) yields

$$\delta\mathbf{u}^{\mathrm{T}}[\mathbf{K}\mathbf{u} + \mathbf{M}\ddot{\mathbf{u}}] = 0. \tag{45}$$

Since the virtual displacements $\delta\mathbf{u}$ are arbitrary, the above equation may be written as

$$\mathbf{K}\mathbf{u} + \mathbf{M}\ddot{\mathbf{u}} = 0. \tag{46}$$

A general solution of Eq. (46) may be written as

$$\mathbf{u} = \phi_k \mathrm{e}^{\mathrm{i}\omega_k t}. \tag{47}$$

Substituting Eq. (47) into Eq. (46) yields

$$[\mathbf{K} - \omega_k^2 \mathbf{M}]\phi_k = 0, \tag{48}$$

where ϕ_k is a set of displacement-type amplitude at the nodes otherwise known as the modal vector and ω_k is the natural frequency associated with the kth mode and $\mathbf{K} = \bigcup_{e=1}^{nel} \mathbf{K}^{(e)}$ is global stiffness matrices which contain contributions from the element stiffness

$$\mathbf{K}_{ab}^{(e)} = \int_{\tilde{A}^{(e)}} [\tilde{\mathbf{B}}_\kappa^{a\mathrm{T}} \tilde{\mathbf{D}}^* \tilde{\mathbf{B}}_\kappa^b + \tilde{\mathbf{B}}_s^{a\mathrm{T}} \tilde{\mathbf{G}}^* \tilde{\mathbf{B}}_s^b] \, \mathrm{d}\tilde{A}, \tag{49}$$

where the rigidity matrices $\tilde{\mathbf{D}}^*$ and $\tilde{\mathbf{G}}^*$ are given in Eq. (34). The $\tilde{\mathbf{B}}_\kappa^a$ is the matrix related to the curvature term and the $\tilde{\mathbf{B}}_s^a$ is the matrix due to assumed transverse shear strains defined in Eqs. (20) and (21). The element mass matrices is provided as consistent and lumped mass matrix forms in the previous section. The global mass matrix is formulated from the element mass such as $\mathbf{M} = \bigcup_{e=1}^{nel} \mathbf{M}^{(e)}$. Note that the subspace iteration method is used to solve the eigenvalue problem in Eq. (48).

7. Numerical examples

In order to investigate the accuracy and reliability of the plate element based on the FE formulation described in the previous sections, five numerical examples are considered. The numerical results are compared with analytical solutions and FE reference solutions which are available in the open literature.

7.1. Square plate

A square plate is used to evaluate the effect of different boundary conditions on the vibrational behaviour of the plate. The geometry of the square plate is illustrated in Fig. 4 (left). The plate has

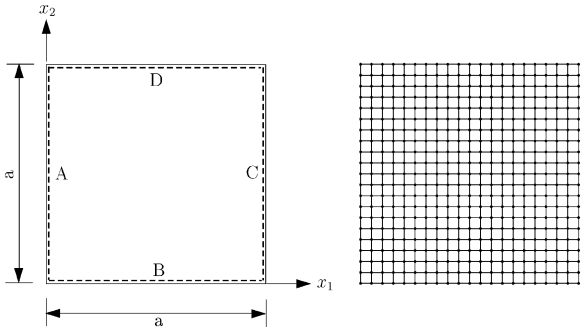

Fig. 4. The geometry of rectangular plate and its FE mesh.

four sides on the $\xi_1 = 0$, $\xi_2 = 0$, $\xi_1 = a$, $\xi_2 = a$ which are denoted as four letters A–B–C–D. The six set of boundary conditions are used in this examples: (a) S-S-S-S, (b) C-C-C-C, (c) C-C-C-F, (d) S-C-S-C, (e) S-C-S-S, (f) S-C-S-F, where S, C and F stand for the simply supported, clamped and free boundary conditions, respectively. In order to compare the present results with the existing reference solutions [18,19], the different values of shear correction factors are employed according to the boundary conditions: (a) S-S-S-S, $k_s = 0.8330$; (b) C-C-C-C, $k_s = 0.8330$; (c) C-C-C-F, $k_s = 0.8601$; (d) S-C-S-C, $k_s = 0.8220$; (e) S-C-S-S, $k_s = 0.8220$; (f) S-C-S-F, $k_s = 0.8220$. Two thickness–span ratios $h/a = 0.01, 0.1$ are used in FE analysis to show the applicability of the present plate element to both thin and thick plates.

In this example, the frequencies are presented in the following form:

$$\Omega_n = w_n a(\rho/G)^{1/2},$$

where a is the side lengths of the plate, ρ is the density of the material and the $G = E/2(1 + v)$ is the shear modulus in which E is the elastic modulus and $v = 0.3$ is the Poisson ratio.

Prior to evaluate the sensitivity of plate frequencies to different boundary conditions, a convergence study is carried out to check the convergence rate of the present plate element. Three uniform FE meshes with 16, 64, 256 four-node elements are used in the convergence study with the boundary of S-S-S-S. From numerical results as shown in Fig. 5, the present plate element shows a good monotonic convergence rate. We therefore decided to use the FE mesh with 400 four-node elements for evaluation of plate frequencies with various boundary conditions. Note that the numerical results with 400 four-node elements can be directly compared to the existing FE reference solution calculated with 100 nine-node FEs [14].

In numerical tests, both consistent and lumped mass matrices are used to calculate natural frequencies and the corresponding modes. The frequencies obtained by using the consistent mass matrix show slightly higher values than those calculated by the lumped mass matrix. The frequencies calculated with the lumped mass matrix in the lower mode have a good agreement with the reference solution [19–21], but the frequencies produced by consistent mass matrix have a better agreement with the reference solution in higher modes. Although the present FE produces a little higher values of frequencies than those calculated by the assumed natural nine-node plate FE described in Ref. [14], it generally has a good agreement with the existing reference solutions [18–24]. In addition, the present element does not show any locking phenomenon with the

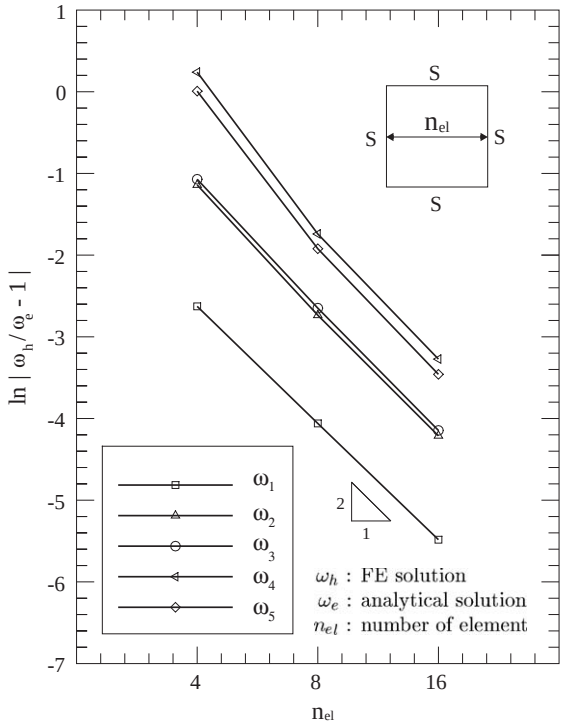

Fig. 5. The rate convergence study with rectangular plate.

stiffness matrix formed by full Gauss integration but on the contrary the numerical results produced by the standard RM plate element denoted as SP4 exhibit serious locking phenomenon in thin plate as described in Table 1. All the numerical results are summarized in Tables 1–6.

7.2. *Parallelogram plate*

As further investigation into the performance of the present element on the rectangular shape plate, a parallelogram plate is used. In this example, we mainly examine the effect of the skewness on the vibrational behaviour of the plate. The numerical analyses are therefore carried out for the angles $0^\circ \leqslant \theta \leqslant 50^\circ$ with the aspect ratio $a/b = 1$. The geometry of parallelogram plate is illustrated in Fig. 6 (left).

The same notation used in the previous example is adopted to denote the boundary condition of the plate and the case S–C–S–C is used in this example. The plate is discretized with a mesh of 400, four-node elements as shown in Fig. 6 (right). The thickness–span ratio $h/a = 0.01$ is used in FE analysis. The resulting frequencies are presented in the following form:

$$\Omega_n = \frac{w_n a^2}{\pi^2}(\rho h/D)^{1/2},$$

Table 1
The parameterized natural frequencies Ω_{mn} of a plate with the S/S/S/S boundary condition

m	n	3D	MC	TC	SP4	ANP9	ANP9a	Pre-a	Pre-b
For the thickness $h/a = 0.1$									
1	1	0.932	0.930	0.963	0.9487	0.9303	0.9303	0.9327	0.9289
2	1	2.226	2.219	2.408	2.2878	2.2198	2.2195	2.2394	2.2165
2	2	3.421	3.406	3.853	3.4896	3.4064	3.4054	3.4381	3.3820
3	1	4.171	4.149	4.816	4.3352	4.1542	4.1510	4.2364	4.1502
3	2	5.239	5.206	6.261	5.3785	5.2102	5.2053	5.2957	5.1560
4	1	—	6.520	8.187	6.9065	6.5425	6.5270	6.7564	6.5244
3	3	6.889	6.834	—	7.0531	6.8414	6.8307	6.9652	6.7122
4	2	7.511	7.446	—	7.8001	7.4673	7.4484	7.6736	7.3645
4	3	—	8.896	—	9.2554	8.9178	8.8892	9.1428	8.6848
5	1	9.268	9.174	—	9.8630	9.2444	9.1928	9.6690	9.1660
5	2	—	9.984	—	10.6256	10.051	9.9924	10.4566	9.8516
4	4	10.89	10.764	—	11.2122	10.796	10.743	11.0955	10.3892
For the thickness $h/a = 0.01$									
1	1		0.0963	0.0963	0.2079	0.0963	0.0963	0.0966	0.0962
2	1		0.2406	0.2408	0.5917	0.2406	0.2406	0.2430	0.2405
2	2		0.3848	0.3853	0.8358	0.3848	0.3847	0.3890	0.3826
3	1		0.4809	0.4816	1.2930	0.4814	0.4810	0.4928	0.4828
3	2		0.6249	0.6261	1.4454	0.6253	0.6247	0.6380	0.6212
4	1		0.8167	0.8187	1.8958	0.8198	0.8179	0.8551	0.8257
3	3		0.8647	—	2.3061	0.8652	0.8639	0.8857	0.8536
4	2		0.9605	—	2.4148	0.9633	0.9609	0.9991	0.9589
4	3		1.1997	—	2.7376	1.2025	1.1988	1.2449	1.1826

Note: 3D: three-dimensional closed-form solution [22]; MC: Reissner–Mindlin thick-plate closed-form solution [21]; TC: thin-plate closed-form solution [20]; SP4: four-node standard plate bending FE solution using consistent mass; ANP9: nine-node assumed strain plate bending FE solution using consistent mass [12,14]; ANP9a: nine-node assumed strain plate bending FE solution using lumped mass [12,14]; Pre-a: present FE solution using consistent mass; Pre-b: present FE solution using lumped mass.

where a is the side length of the plate, ρ is the density of material and $D = Eh^3/12(1-\nu^2)$ is the flexural rigidity of the plate in which E is the elastic modulus and $\nu = 0.3$ is the Poisson ratio.

From numerical results, the modes are divided into symmetric and antisymmetric groups in accordance with the local axis (ξ_i) induced by the skewness. It appears that the skewness intensifies the rigidity of the plate and the higher frequencies are therefore detected in the plate with severer skewness. Although there is some difference between the present FE solution and reference solution [25] in case of plate with higher skewness, the solutions calculated by the consistent mass matrix have a good agreement with the reference solutions as shown in Table 7. The maximum difference of 4.31% is observed between the frequencies calculated by using consistent matrix and reference solutions with the highest skewness. The mode shapes are also found to be greatly influenced by the degree of skewness. The mode shapes of the plate according to various skewness are illustrated in Fig. 7.

Table 2
The parameterized natural frequencies Ω_{mn} of a plate with the C/C/C/C boundary condition

m	n	MC	TC	SP4	ANP9	ANP9a	Pre-a	Pre-b
For the thickness $h/a = 0.1$								
1	1	1.594	1.756	1.6345	1.5913	1.5912	1.5962	1.5885
2	1	3.046	3.581	3.1349	3.0406	3.0397	3.0683	3.0335
2	2	4.285	5.280	4.3717	4.2653	4.2631	4.2999	4.2243
3	1	5.035	6.421	5.2315	5.0341	5.0289	5.1275	5.0172
3	2	5.078	6.451	5.2810	5.0817	5.0763	5.1767	5.0662
4	1			6.2693	6.0891	6.0817	6.1745	6.0039
3	3	—	—	7.8016	7.4459	7.4258	7.6621	7.3928
4	2	—	—	7.9044	7.6934	7.6788	7.8053	7.5120
4	3	—	—	8.6082	8.2911	8.2675	8.4836	8.1330
5	1	—	—	8.6884	8.3669	8.3427	8.5642	8.2115
5	2	—	—	10.0453	9.7322	9.6978	9.9295	9.4216
For the thickness $h/a = 0.01$								
1	1	0.1754	0.1756	0.4531	0.1754	0.1754	0.1765	0.1756
2	1	0.3576	0.3581	0.9421	0.3576	0.3575	0.3635	0.3592
2	2	0.5274	0.5280	1.2734	0.5268	0.5265	0.5359	0.5260
3	1	0.6402	0.6421	1.7710	0.6415	0.6407	0.6634	0.6484
3	2	0.6432	0.6432	1.7733	0.6446	0.6438	0.6666	0.6516
4	1	—	—	1.9885	0.8034	0.8021	0.8267	0.8026
3	3	—	—	2.5319	1.0296	1.0261	1.0876	1.0472
4	2	—	—	2.9271	1.0705	1.0679	1.1052	1.0614
4	3	—	—	3.0781	1.1818	1.1776	1.2395	1.1853
5	1	—	—	3.0826	1.1868	1.1825	1.2448	1.1908
5	2	—	—	3.4802	1.4436	1.4373	1.5095	1.4282

Note: MC: reference solution using the Rayleigh–Ritz method [19]; TC: reference solution using the Rayleigh–Ritz method (thin plate theory) [20]; SP4: four-node standard plate bending FE solution using consistent mass; ANP9: nine-node assumed strain plate bending FE solution using consistent mass [12,14]; ANP9a: nine-node assumed strain plate bending FE solution using lumped mass [12,14]; Pre-a: present FE solution using consistent mass; Pre-b: present FE solution using lumped mass.

7.3. Circular plate

A circular plate with clamped boundaries is analyzed. The entire plate is used to examine the free vibration behaviour of the plate. The geometry of the plate is illustrated in Fig. 8 (left) and it is discretized with a mesh of 432, four-node elements as shown in Fig. 8 (right).

Two thickness–span ratios $h/2r = 0.01$ and 0.1 are used in this study. The resulting frequencies are presented in the following form:

$$\Omega_n = w_n r^2 (\rho h/D)^{1/2},$$

where r is the radius of the circular plate, ρ is the density of material and the $D = Eh^3/12(1-v^2)$ is the flexural rigidity of the plate in which E is the elastic modulus and $v = 0.3$ is the Poisson ratio. From numerical results, asymmetric and axisymmetric vibration modes are detected and multiple frequencies are obtained from the axisymmetric modes. It is shown that there is minor numerical

Table 3
The parameterized natural frequencies Ω_n of a plate with the C/C/C/F boundary condition

n	MC	TC	SP4	ANP9	ANP9a	Pre-a	Pre-b
For the thickness $h/a = 0.1$							
1	1.089	1.171	1.1167	1.0807	1.0807	1.0846	1.0810
2	1.785	1.953	1.7840	1.7440	1.7438	1.7473	1.7326
3	2.673	3.094	2.7616	2.6577	2.6569	2.6863	2.6597
4	3.216	3.744	3.2961	3.1979	3.1967	3.2207	3.1660
5	3.318	3.938	3.3778	3.2912	3.2902	3.3125	3.2646
6	4.615	5.699	4.6664	4.5605	4.5579	4.5884	4.4827
7			4.9540	4.7378	4.7328	4.8303	4.7331
8	—	—	5.4645	5.2521	5.2457	5.3367	5.1834
9	—	—	5.5060	5.3185	5.3129	5.3968	5.2647
10	—	—	6.5933	6.4016	6.3925	6.4768	6.2503
11	—	—	6.6272	6.4539	6.4456	6.5242	6.3100
12	—	—	7.5419	7.1630	7.1454	7.3710	7.1204
13	—	—	8.0300	7.6879	7.6669	7.8748	7.5637
14	—	—	8.0925	7.7092	7.6851	7.9108	7.5749
For the thickness $h/a = 0.01$							
1	0.1171	0.1171	0.3214	0.1166	0.1166	0.1174	0.1171
2	0.1951	0.1953	0.4589	0.1949	0.1949	0.1960	0.1943
3	0.3093	0.3094	0.8780	0.3082	0.3081	0.3143	0.3110
4	0.3740	0.3744	0.9493	0.3738	0.3736	0.3789	0.3721
5	0.3931	0.3938	0.9564	0.3924	0.3923	0.3984	0.3924
6	0.5695	0.5699	1.2923	0.5678	0.5674	0.5770	0.5630
7	—	—	1.7322	0.5963	0.5955	0.6188	0.6057
8	—	—	1.7779	0.6556	0.6547	0.6749	0.6536
9	—	—	1.7888	0.6835	0.6825	0.7053	0.6872
10	—	—	2.0061	0.8417	0.8402	0.8636	0.8311
11	—	—	2.0141	0.8605	0.8591	0.8844	0.8539
12	—	—	2.5609	0.9833	0.9800	1.0422	1.0048
13	—	—	2.8977	1.0400	1.0361	1.0914	1.0386
14	—	—	2.9328	1.0720	1.0684	1.1296	1.0844

Note: MC: reference solution using the Rayleigh–Ritz method [19]; TC: reference solution using the Rayleigh–Ritz method (thin plate theory) [20]; SP4: four-node standard plate bending FE solution using consistent mass; ANP9: nine-node assumed strain plate bending FE solution using consistent mass [12,14]; ANP9a: nine-node assumed strain plate bending FE solution using lumped mass [12,14]; Pre-a: present FE solution using consistent mass; Pre-b: present FE solution using lumped mass.

difference between the reference solution [1] and the present result for the thickness–span ratio $h/2r = 0.01$. More specifically, some intermediate frequencies are calculated in the FE analysis. However, the frequencies obtained from the present plate element show a very good agreement with analytical solution based on Mindlin theory [26] and the higher order FE solutions [12,14] in overall modes. In case of the thickness–span ratio $h/2r = 0.1$, the present result have a good agreement with the reference solution [26] based on Mindlin plate theory. The natural frequencies

Table 4
The parameterized natural frequencies Ω_n of a plate with the S/C/S/C boundary condition

n	MC	TC	FS	SP4	ANP9	ANP9a	Pre-a	Pre-b
For the thickness $h/a = 0.1$								
1	1.302	1.413	1.300	1.3368	1.3002	1.3002	1.3105	1.3047
2	2.398	2.671	2.394	2.4704	2.3946	2.3941	2.4234	2.3981
3	2.888	3.383	2.885	2.9930	2.8861	2.8852	2.9412	2.9086
4	3.852	4.615	3.839	3.9535	3.8410	3.8394	3.9070	3.8408
5	4.237	4.988	4.232	4.4247	4.2362	4.2328	4.3388	4.2499
6	4.939	6.299	4.936	5.1792	4.9444	4.9394	5.1044	4.9957
7	—	—	—	5.6523	5.4626	5.4571	5.5886	5.4389
8	—	—	—	6.0156	5.7979	5.7913	5.9597	5.7978
9	—	—	—	6.9543	6.5768	6.5611	6.8351	6.5998
10	—	—	—	7.4829	7.2296	7.2173	7.4326	7.1581
11	—	—	—	7.7554	7.3315	7.3119	7.6691	7.4000
12	—	—	—	7.9603	7.6051	7.5854	7.8722	7.5529
13	—	—	—	8.4899	8.0972	8.0746	8.4274	8.0822
14	—	—	—	9.5323	9.1558	9.1256	9.4747	8.9960
For the thickness $h/a = 0.01$								
1	0.1411	0.1413	0.1411	0.3524	0.1411	0.1411	0.14194	0.1413
2	0.2668	0.2671	0.2668	0.6589	0.2668	0.2668	0.26938	0.2665
3	0.3377	0.3383	0.3376	0.8961	0.3378	0.3377	0.34378	0.3398
4	0.4608	0.4615	0.4604	1.0767	0.4607	0.4604	0.46757	0.4594
5	0.4979	0.4988	0.4977	1.3268	0.4984	0.4980	0.50982	0.4993
6	0.6279	0.6299	0.6279	1.6008	0.6295	0.6287	0.65171	0.6372
7	—	—	—	1.7467	0.6827	0.6820	0.69726	0.6782
8	—	—	—	1.8652	0.7539	0.7529	0.77634	0.7544
9	—	—	—	2.2363	0.8321	0.8301	0.86727	0.8373
10	—	—	—	2.3266	0.9725	0.9705	1.00083	0.96280
11	—	—	—	2.5142	1.0080	1.0052	1.04474	1.00188
12	—	—	—	2.9108	1.0190	1.0158	1.07782	1.03796
13	—	—	—	2.9875	1.1460	1.1416	1.20343	1.15188
14	—	—	—	2.9995	1.2690	1.2623	1.33958	1.27054

Note: MC: reference solution using the Rayleigh–Ritz method [19]; TC: thin-plate closed-form solution [20]; FS: the Reissner–Mindlin finite strip solution [24]; SP4: four-node standard plate bending FE solution using consistent mass; ANP9: nine-node assumed strain plate bending FE solution using consistent mass [12,14]; ANP9a: nine-node assumed strain plate bending FE solution using lumped mass [12,14]; Pre-a: present FE solution using consistent mass; Pre-b: present FE solution using lumped mass.

are presented in Table 8 where the FE reference solution denoted as ANS9 is obtained by using the lumped mass matrix. The mode shapes of the circular plate are illustrated in Fig. 9.

7.4. Elliptical plates

The vibration characteristics of elliptical plates with aspect ratios $a/b = 2$, 3 and 4 are investigated in this example. The geometry of the plate is presented in Fig. 10 (left).

Table 5
The parameterized natural frequencies Ω_n of a plate with the S/C/S/S boundary condition

n	MC	TC	FS	SP4	ANP9	ANP9a	Pre-a	Pre-b
For the thickness $h/a = 0.1$								
1	1.092	1.154	1.092	1.1181	1.0919	1.0918	1.09783	1.09307
2	2.298	2.521	2.296	2.3689	2.2969	2.2965	2.32367	2.29958
3	2.543	2.862	2.542	2.6305	2.5425	2.5420	2.58119	2.55357
4	3.616	4.203	3.611	3.7111	3.6121	3.6108	3.66627	3.60518
5	4.187	4.893	4.184	4.3766	4.1892	4.1859	4.29109	4.20344
6	4.543	5.525	4.541	4.7587	4.5475	4.5434	4.67715	4.57955
7	—	—	—	5.5095	5.3267	5.3216	5.44619	5.30131
8	—	—	—	5.6941	5.4967	5.4910	5.63367	5.48263
9	—	—	—	6.9291	6.5521	6.5365	6.81023	6.57605
10	—	—	—	7.2644	6.9368	6.9192	7.21111	6.94678
11	—	—	—	7.3383	7.0252	7.0137	7.23479	6.98343
12	—	—	—	7.8774	7.5256	7.5063	7.78957	7.47468
13	—	—	—	8.1478	7.7762	7.7554	8.07188	7.74373
14	—	—	—	9.3914	9.0236	8.9942	9.33228	8.86266
For the thickness $h/a = 0.01$								
1	0.1153	0.1154	0.1153	0.2679	0.1153	0.1153	0.1158	0.1153
2	0.2521	0.2521	0.2519	0.6171	0.2519	0.2519	0.2544	0.2517
3	0.2858	0.2862	0.2858	0.7347	0.2859	0.2858	0.2897	0.2866
4	0.4199	0.4203	0.4195	0.9447	0.4197	0.4195	0.4249	0.4178
5	0.4889	0.4893	0.4883	1.3059	0.4890	0.4886	0.5004	0.4902
6	0.5533	0.5525	0.5513	1.5109	0.5522	0.5516	0.5683	0.5562
7	—	—	—	1.5132	0.6518	0.6511	0.6653	0.6474
8	—	—	—	1.6450	0.6862	0.6854	0.7032	0.6840
9	—	—	—	2.0543	0.8255	0.8235	0.8607	0.8311
10	—	—	—	2.3142	0.9159	0.9136	0.9398	0.9048
11	—	—	—	2.4579	0.9162	0.9142	0.9621	0.9277
12	—	—	—	2.5996	0.9840	0.9815	1.0204	0.9789
13	—	—	—	2.6977	1.0510	1.0478	1.0968	1.0511
14	—	—	—	2.8520	1.2450	1.2404	1.2895	1.2240

Note: MC: reference solution using the Rayleigh–Ritz method [19]; TC: thin-plate closed-form solution [20]; FS: the Reissner–Mindlin finite strip solution [24]; SP4: four-node standard plate bending FE solution using consistent mass; ANP9: nine-node assumed strain plate bending FE solution using consistent mass [12,14]; ANP9a: nine-node assumed strain plate bending FE solution using lumped mass [12,14]; Pre-a: present FE solution using consistent mass; Pre-b: present FE solution using lumped mass.

The thickness–span ratio is taken as $h/2b = 0.01$ and 400 FEs as illustrated in Fig. 10 (right) are used in analysis. The resulting frequencies are presented in the following form:

$$\Omega_n = w_n a^2 (\rho h/D)^{1/2},$$

where a is the radius of the elliptical plates in the x_1 direction, ρ is the density of material and $D = Eh^3/12(1-\nu^2)$ is the flexural rigidity of the plate in which E is the elastic modulus and $\nu = 0.3$ is the Poisson ratio.

Table 6
The parameterized natural frequencies Ω_n of a plate with the S/C/S/F boundary condition

n	MC	TC	FS	SP4	ANP9	ANP9a	Pre-a	Pre-b
For the thickness $h/a = 0.1$								
1	0.603	0.619	0.598	0.6148	0.5977	0.5977	0.6001	0.5984
2	1.495	1.613	1.483	1.5185	1.4836	1.4835	1.4949	1.4827
3	1.900	2.035	1.884	1.9639	1.8848	1.8845	1.9097	1.8927
4	2.744	3.075	2.720	2.7945	2.7220	2.7214	2.7555	2.7178
5	3.073	3.533	3.057	3.1689	3.0595	3.0584	3.1107	3.0585
6	3.855	4.421	3.827	4.0351	3.8329	3.8299	3.9354	3.8600
7	—	—	—	4.3051	4.1892	4.1872	4.2601	4.1642
8	—	—	—	4.7520	4.5709	4.5671	4.6775	4.5676
9	—	—	—	5.3998	5.1551	5.1489	5.3070	5.1547
10	—	—	—	6.0912	5.9013	5.8948	6.0373	5.8436
11	—	—	—	6.3793	6.1497	6.1415	6.3133	6.0947
12	—	—	—	6.6341	6.2367	6.2218	6.4988	6.2825
13	—	—	—	7.2435	6.8765	6.8598	7.1360	6.8696
14	—	—	—	7.9615	7.6122	7.5885	7.9114	7.5613
For the thickness $h/a = 0.01$								
1	0.0622	0.0619	0.0619	0.1520	0.0619	0.0619	0.0620	0.0619
2	0.1612	0.1613	0.1611	0.3578	0.1612	0.1612	0.1620	0.1606
3	0.2045	0.2035	0.2033	0.5656	0.2034	0.2033	0.2057	0.2038
4	0.3075	0.3075	0.3070	0.6765	0.3071	0.3070	0.3099	0.3056
5	0.3528	0.3533	0.3526	0.9025	0.3528	0.3527	0.3580	0.3516
6	0.4438	0.4421	0.4413	1.0964	0.4420	0.4417	0.4536	0.4449
7	—	—	—	1.2744	0.5024	0.5021	0.5094	0.4975
8	—	—	—	1.3473	0.5454	0.5449	0.5571	0.5439
9	—	—	—	1.6300	0.6411	0.6402	0.6606	0.6399
10	—	—	—	1.7518	0.7438	0.7430	0.7593	0.7344
11	—	—	—	1.8819	0.7786	0.7768	0.8119	0.7820
12	—	—	—	2.2667	0.7911	0.7899	0.8142	0.7872
13	—	—	—	2.2903	0.8809	0.8788	0.9161	0.8818
14	—	—	—	2.3471	1.0288	1.0252	1.0638	1.0148

Note: MC: reference solution using the Rayleigh–Ritz method [19]; TC: thin-plate closed-form solution [20]; FS: the Reissner–Mindlin finite strip solution [24]; SP4: four-node standard plate bending FE solution using consistent mass; ANP9: nine-node assumed strain plate bending FE solution using consistent mass [12,14]; ANP9a: nine-node assumed strain plate bending FE solution using lumped mass [12,14]; Pre-a: present FE solution using consistent mass; Pre-b: present FE solution using lumped mass.

From numerical results, the frequencies calculated by using the present plate element show a good agreement with a reference solution [27] except for some difference in the higher mode. The mode shape up to the third mode does not change regardless of the different aspect ratios but it has been greatly effected by the aspect ratio (a/b) of the plate in higher modes. In particular, the larger aspect ratio produces larger numbers of waves dominantly in the x_1 direction. Both consistent and lumped mass matrix are used in FE analysis and the maximum error of 2.13% is

Table 7
The parameterized natural frequencies Ω_n of parallelogram plate

	Mode n									
a/b	θ		1	2	3	4	5	6	7	8
	0	refa	2.933	5.548	7.024	9.586	10.361	13.080	14.210	15.690
		Pre-a	2.947	5.593	7.138	9.708	10.586	13.531	14.477	16.119
		Pre-b	2.934	5.534	7.056	9.539	10.367	13.229	14.082	15.664
	5	refa	2.953	5.570	7.084	9.557	10.500	13.180	14.140	15.870
		Pre-a	2.966	5.615	7.197	9.684	10.716	13.636	14.415	16.297
		Pre-b	2.953	5.555	7.114	9.513	10.497	13.331	14.019	15.836
	10	refa	3.014	5.641	7.266	9.529	10.860	13.500	14.030	16.340
		Pre-a	3.025	5.682	7.375	9.658	11.063	13.956	14.307	16.751
		Pre-b	3.011	5.621	7.290	9.483	10.839	13.644	13.907	16.270
	15	refa	3.121	5.765	7.579	9.552	11.390	13.980	14.080	16.960
		Pre-a	3.125	5.800	7.680	9.693	11.584	14.256	14.512	17.384
		Pre-b	3.111	5.737	7.591	9.511	11.348	13.850	14.186	16.870
	20	refa	3.276	5.955	8.040	9.699	12.100	14.050	14.910	17.750
		Pre-a	3.275	5.981	8.127	9.818	12.274	14.319	15.336	18.187
		Pre-b	3.260	5.914	8.032	9.630	12.021	13.902	14.991	17.628
	25	refa	3.497	6.226	8.678	9.949	13.000	14.300	16.100	18.800
		Pre-a	3.483	6.237	8.742	10.057	13.162	14.529	16.478	19.209
		Pre-b	3.466	6.166	8.639	9.859	12.884	14.096	16.102	18.594
	30	refa	3.797	6.598	9.539	10.300	14.100	14.700	17.800	19.600
		Pre-a	3.765	6.591	9.565	10.436	14.298	14.921	17.991	20.415
		Pre-b	3.746	6.514	9.450	10.224	13.986	14.464	17.561	19.564
	35	refa	4.203	7.104	10.700	10.900	15.400	15.700	19.600	20.900
		Pre-a	4.142	7.071	10.658	10.988	15.537	15.761	19.830	21.356
		Pre-b	4.121	6.984	10.527	10.757	15.046	15.404	19.232	20.566
	40	refa	4.753	7.791	11.800	12.200	16.400	17.600	21.300	23.300
		Pre-a	4.649	7.720	11.768	12.117	16.444	17.676	21.493	23.564
		Pre-b	4.625	7.621	11.509	11.962	15.905	17.256	20.599	22.918
	45	refa	5.510	8.74	12.900	14.400	17.800	20.300	23.000	27.300
		Pre-a	5.341	8.605	12.856	14.088	17.749	20.233	23.129	27.307
		Pre-b	5.311	8.488	12.559	13.899	17.145	19.724	22.067	26.493
	50	refa	6.590	10.100	14.600	17.400	19.700	24.000	25.300	32.000
		Pre-a	6.306	9.835	14.387	16.797	19.642	23.723	25.336	31.449
		Pre-b	6.269	9.693	14.034	16.547	18.952	23.067	24.121	29.710

Note: refa: reference solution using the Ritz method (thin plate theory) [25]; Pre-a: present FE solution using consistent mass; Pre-b: present FE solution using lumped mass.

observed between the frequencies calculated by using consistent and lumped mass matrices in case of the aspect ratio $a/b = 4$. The natural frequencies are summarized in Table 9 and the mode shapes refer to the illustrations in Ref. [14].

7.5. Triangular plate

A triangular cantilever plate is considered to investigate the performance of the present plate element in the cantilever situation with various skewnesses. The geometry of the plate is varied

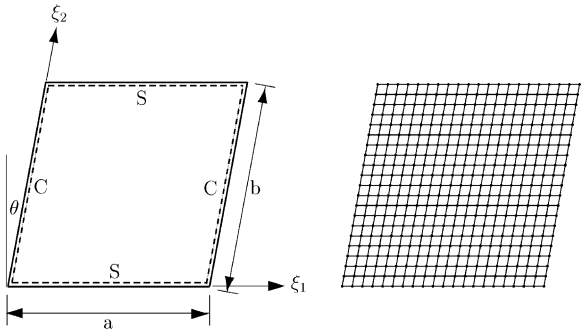

Fig. 6. The geometry of parallelogram plate and its FE mesh.

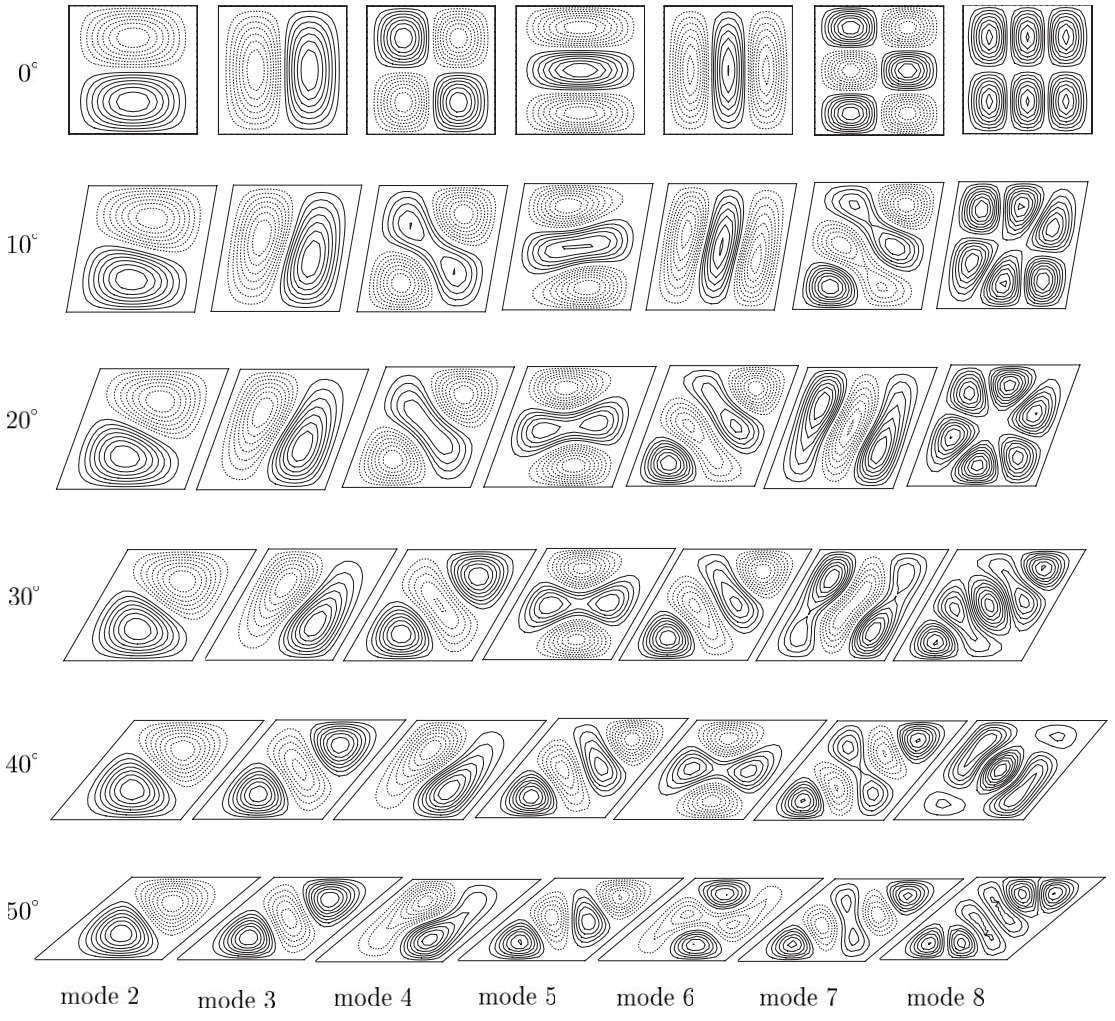

Fig. 7. Mode shapes of a parallelogram plate with the aspect ratio: $h/a = 0.01$.

Table 8
The parameterized natural frequencies Ω_n of a clamped circular plate

	Aspect ratio $h/2r = 0.01$					Aspect ratio $h/2r = 0.1$		
n	AS1	AS2	ANS9	Pre-a	Pre-b	AS3	Pre-a	Pre-b
1	10.2158	10.216	10.2129	10.2572	10.2196	9.240	9.2605	9.2277
2	21.2600	21.260	21.2311	21.4981	21.3149	17.834	17.9469	17.8010
—	—	—	—	—	—	—	—	—
3	34.8800	34.877	34.7816	35.3941	34.9217	27.214	27.0345	26.6801
—	—	—	34.7915	35.5173	34.9411	—	27.6566	27.2246
4	39.7710	39.771	39.6766	40.8975	40.2339	30.211	30.3221	29.8562
5	51.0400	51.030	50.8348	52.2054	50.9826	37.109	37.2579	36.3966
—	—	—	—	—	—	—	—	—
6	60.8200	60.829	60.6761	63.2397	61.4506	42.409	43.2702	42.1089
—	—	—	—	—	—	—	—	—
7	69.6659	69.666	69.3028	71.7426	69.2707	47.340	47.7074	46.0596
—	—	—	69.3379	72.0375	69.4915	—	47.8028	46.0985
8	84.5800	84.583	84.2999	88.1498	84.6280	54.557	56.0625	53.9332
—	—	—	84.3835	89.3007	85.3834	—	57.1311	54.7720
9	111.010	89.104	88.9848	94.6775	90.0831	56.682	58.1458	55.8268
10	140.108	90.739	90.2078	94.7423	—	57.793	58.7867	55.8602
—		—	—	—	90.6341	—	—	—
11		111.021	110.563	117.4438	110.9489	66.667	69.2908	65.5682
—		—	—	—	—	—	—	65.7435
12		114.213	113.489	121.0943	113.0738	68.396	70.2640	65.7435
—		—	113.502	121.1140	113.1239	—	70.5168	65.7772
13		120.079	119.848	130.3322	122.9492	70.473	73.1408	69.1471
—		—	—	—	—	—	—	—
14		140.108	139.222	149.1776	138.4807	78.733	81.6580	75.4313
—		—	—	—	—	—		—
15		153.815	139.228	151.4207	139.0212	83.937	82.5909	76.4241
—		—	139.376	151.4207	139.5913		—	77.4281

Note: AS1: analytical solution [1]; AS2: analytical solution ($h/2r = 0$) [26]; ANP9a: nine-node assumed strain plate bending FE solution using lumped mass [12,14]; AS3: analytical solution [26]; Pre-a: present FE solution using consistent mass; Pre-b: present FE solution using lumped mass; — multiple frequencies associated with axisymmetrix modes.

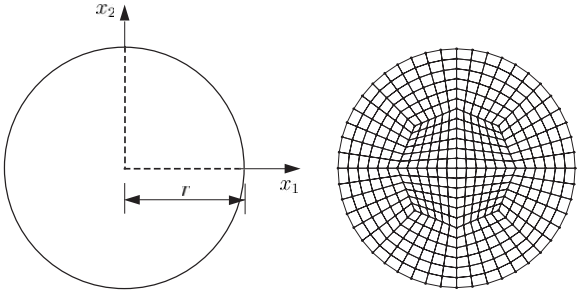

Fig. 8. The geometry of circular plate and its FE mesh.

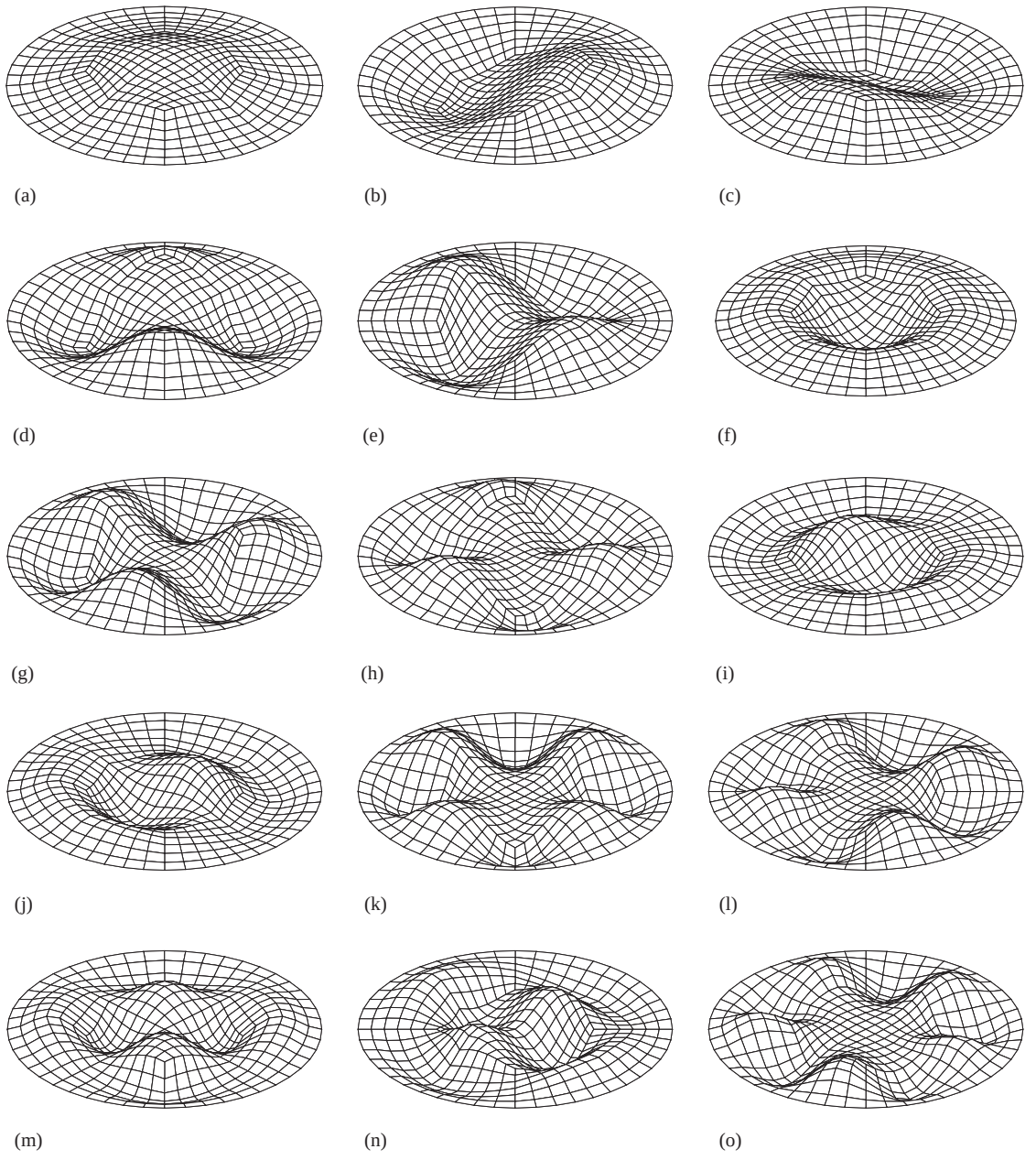

Fig. 9. Mode shapes of a circular plate with the aspect ratio $h/a = 0.01$: (a) mode 1–(o) mode 15.

with the parameters a, b, θ as shown in Fig. 11 (left). Two thickness–span ratios $h/a = 0.001$ and 0.2 are used with the aspect ratio $b/a = 1.0$. Six skew angles such as $\theta = 90^\circ$, 105°, 120°, 135°, 150°, 165°, are considered and it is discretized with a mesh of 398, four-node element shown in Fig. 11 (right).

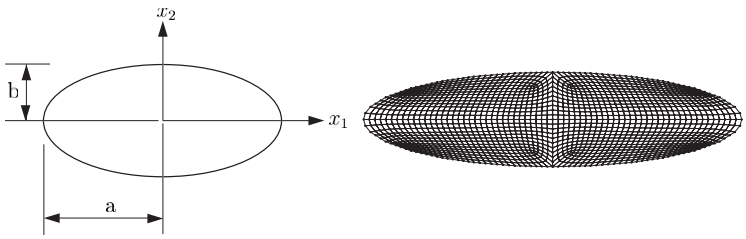

Fig. 10. The geometry of elliptical plate and its FE mesh.

Table 9
The parameterized natural frequencies Ω_n of clamped elliptical plates

	$a/b = 2$			$a/b = 3$			$a/b = 4$		
n	ref	Pre-a	Pre-b	ref	Pre-a	Pre-b	ref	Pre-a	Pre-b
1	27.4773	27.4835	27.4450	56.8995	56.8426	56.7428	97.5984	96.6481	96.4697
2	39.4976	39.5436	39.4363	71.5902	71.2823	71.1019	115.608	113.3580	113.0638
3	55.9773	56.2277	55.9592	90.2380	89.7835	89.4269	137.269	134.0962	133.5773
4	69.8557	70.0237	69.7234	113.266	112.2233	111.5923	164.325	158.1555	157.3216
5	77.0443	77.6159	77.0353	140.746	139.1438	138.0660	195.340	186.5070	185.1886
6	88.0472	87.6141	87.1306	150.089	149.5870	148.5705	255.095	218.9070	216.9055
7	—	103.8727	102.7483	—	170.6068	168.8583	—	254.3643	252.6294
8	—	109.4776	108.5877	—	171.9638	170.6857	—	256.0217	253.0590
9	—	132.5737	131.4208	—	198.8995	196.9245	—	279.7629	277.7079
10	—	135.0869	133.0942	—	206.8869	204.1486	—	297.6035	293.3309
11	—	135.3557	133.8865	—	228.6011	225.8830	—	311.3225	308.3346
12	—	155.5869	154.1045	—	247.9671	243.8796	—	343.0278	337.4480
13	—	165.6212	163.2066	—	262.5009	258.6107	—	344.3824	340.1423
14	—	171.3334	168.0218	—	286.4414	282.5174	—	380.8356	375.6637
15	—	183.3699	181.0090	—	293.9078	287.9568	—	394.6097	386.3833

Note: ref: reference solution using the Rayleigh–Ritz method [27]; Pre-a: present solution using consistent mass; Pre-b: present solution using lumped mass.

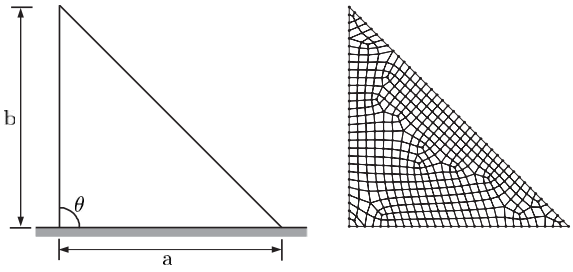

Fig. 11. The geometry of triangular plate and its FE mesh.

In this example, a frequency parameter Ω is used as

$$\Omega_n = \frac{w_n a^2}{\pi^2}(\rho h/D)^{1/2},$$

where a is the side length with clamped boundary, ρ is the density of material and the $D = Eh^3/12(1-v^2)$ is the flexural rigidity of the plate in which E is the elastic modulus and $v = 0.3$ is the Poisson ratio.

The frequencies calculated by using the present plate element with the thickness–span ratio $h/a = 0.001$ show a good agreement with reference solutions [28–31]. In particular, the present solution with consistent mass matrix is found to be very close to the reference solution [30] which uses a special function representing singularity at the corner of thin skewed triangular plate. The plate has similar frequencies regardless of the different values of skew angle in the lower mode. However, the greater skewness triggers some difference in the higher mode. In particular, a large

Table 10
The parameterized natural frequencies Ω_n of triangular plates with the aspect ratio $h/a = 0.001$

	Mode n									
a/b	θ		1	2	3	4	5	6	7	8
	90	refa	0.624	2.336	3.373	5.665	7.547	—	—	—
		refb	0.588	2.318	3.239	5.540	7.518	—	—	—
		refc	0.624	2.377	3.308	5.689	7.743	—	—	—
		refd	0.625	2.377	3.310	5.689	7.743	—	—	—
		Pre-a	0.624	2.379	3.317	5.724	7.794	10.200	11.453	13.801
		Pre-b	0.623	2.362	3.273	5.627	7.663	9.828	11.149	13.428
	105	refa	0.587	2.140	3.441	5.271	6.976	—	—	—
		refc	0.584	2.181	3.409	5.280	7.264	—	—	—
		refd	0.586	2.182	3.412	5.279	7.263	—	—	—
		Pre-a	0.583	2.181	3.413	5.303	7.289	10.095	11.468	13.856
		Pre-b	0.583	2.164	3.361	5.180	7.181	9.656	11.164	13.358
	120	refa	0.584	2.138	3.642	5.486	6.831	—	—	—
		refc	0.576	2.174	3.639	5.511	7.108	—	—	—
		refd	0.578	2.178	3.657	5.518	7.109	—	—	—
		Pre-a	0.575	2.174	3.638	5.534	7.139	10.477	11.873	14.937
		Pre-b	0.575	2.160	3.585	5.409	7.042	10.156	11.503	14.422
	135	refa	0.605	2.327	4.141	6.378	7.393	—	—	—
		refc	0.590	2.329	4.137	6.381	7.602	—	—	—
		refd	0.593	2.335	4.222	6.487	7.609	—	—	—
		Pre-a	0.588	2.324	4.126	6.381	7.614	11.224	13.588	15.815
		Pre-b	0.587	2.312	4.070	6.212	7.498	10.989	13.053	15.193
	150	refc	0.617	2.576	5.376	7.524	10.285	—	—	—
		refd	0.636	2.618	5.521	8.254	10.395	—	—	—
		Pre-a	0.613	2.564	5.353	7.460	10.306	12.942	17.015	20.289
		Pre-b	0.613	2.556	5.263	7.278	9.968	12.767	16.483	19.207

Note: refa: FE reference solution [28]; refb: experimental solution [29]; refc: reference solution using the Rayleigh–Ritz method with corner function [30]; refd: reference solution using the pb2 Rayleigh–Ritz method (Mindlin plate theory) [31]; Pre-a: present FE solution using consistent mass; Pre-b: present FE solution using lumped mass.

Table 11
The parameterized natural frequencies Ω_n of triangular plates with the aspect ratio $h/a = 0.2$

	Mode n								
a/b	θ		1	2	3	4	5	6	7	8
	90	refa	0.582	1.900	2.408	3.936	—	—	—	—
		refb	0.581	1.901	2.410	—	—	—	—	—
		Pre-a	0.582	1.915	2.428	3.984	5.018	5.944	6.670	7.889
		Pre-b	0.582	1.906	2.411	3.946	4.966	5.841	6.581	7.721
	105	refa	0.544	1.771	2.386	3.628	—	—	—	—
		refb	0.543	1.770	2.388	—	—	—	—	—
		Pre-a	0.545	1.764	2.420	3.608	4.820	5.431	6.719	7.195
		Pre-b	0.545	1.755	2.401	3.568	4.774	5.316	6.632	7.032
	120	refa	0.533	1.772	2.419	3.565	—	—	—	—
		refb	0.532	1.769	2.419	—	—	—	—	—
		Pre-a	0.532	1.773	2.437	3.591	4.765	5.323	6.774	7.126
		Pre-b	0.532	1.765	2.417	3.558	4.721	5.236	6.692	7.005
	135	refa	0.540	1.885	2.489	3.674	—	—	—	—
		refb	0.538	1.881	2.482	—	—	—	—	—
		Pre-a	0.541	1.884	2.518	3.748	4.740	5.292	6.897	7.141
		Pre-b	0.540	1.878	2.496	3.714	4.683	5.242	6.802	7.061
	150	refa	0.559	2.059	2.396	3.590	—	—	—	—
		refb	0.555	2.047	2.386	—	—	—	—	—
		Pre-a	0.559	2.095	2.483	3.910	4.517	5.763	6.710	7.802
		Pre-b	0.559	2.091	2.453	3.881	4.485	5.707	6.627	7.737
	165	refa	0.599	1.495	2.267	2.275	—	—	—	—
		refb	0.588	1.598	2.214	—	—	—	—	—
		Pre-a	0.585	1.662	2.251	2.824	4.190	4.761	5.834	7.412
		Pre-b	0.585	1.651	2.249	2.805	4.145	4.750	5.749	7.345

Note: refa: reference solution using the pb2 Rayleigh–Ritz method (Mindlin plate theory) [31]; refb: FE solution (higher-order Mindlin plate theory) [32]; Pre-a: present FE solution using consistent mass; Pre-b: present FE solution using lumped mass.

drop in frequency is detected after the third mode of the plate. It is also observed that the plate with the thickness–span ratio $h/a = 0.2$ produces lower frequencies than those calculated with the $h/a = 0.001$ due to the effects of shear deformation and rotatory inertia. In general, the present FE solution has a good agreement with other reference solutions in both very thin and thick cases. The natural frequencies are summarized in Tables 10 and 11. The mode shapes of the triangular plate with the aspect ratio $h/a = 0.001$ are illustrated in Fig. 12.

8. Conclusions

The assumed natural strain four-node plate element is developed to assess the vibrational behaviour of plate structures. In particular, the explicit expression of the assumed natural transverse shear strains is provided. The accuracy and efficiency of the proposed plate FE formulation are tested by five numerical examples. From the numerical results, the present plate

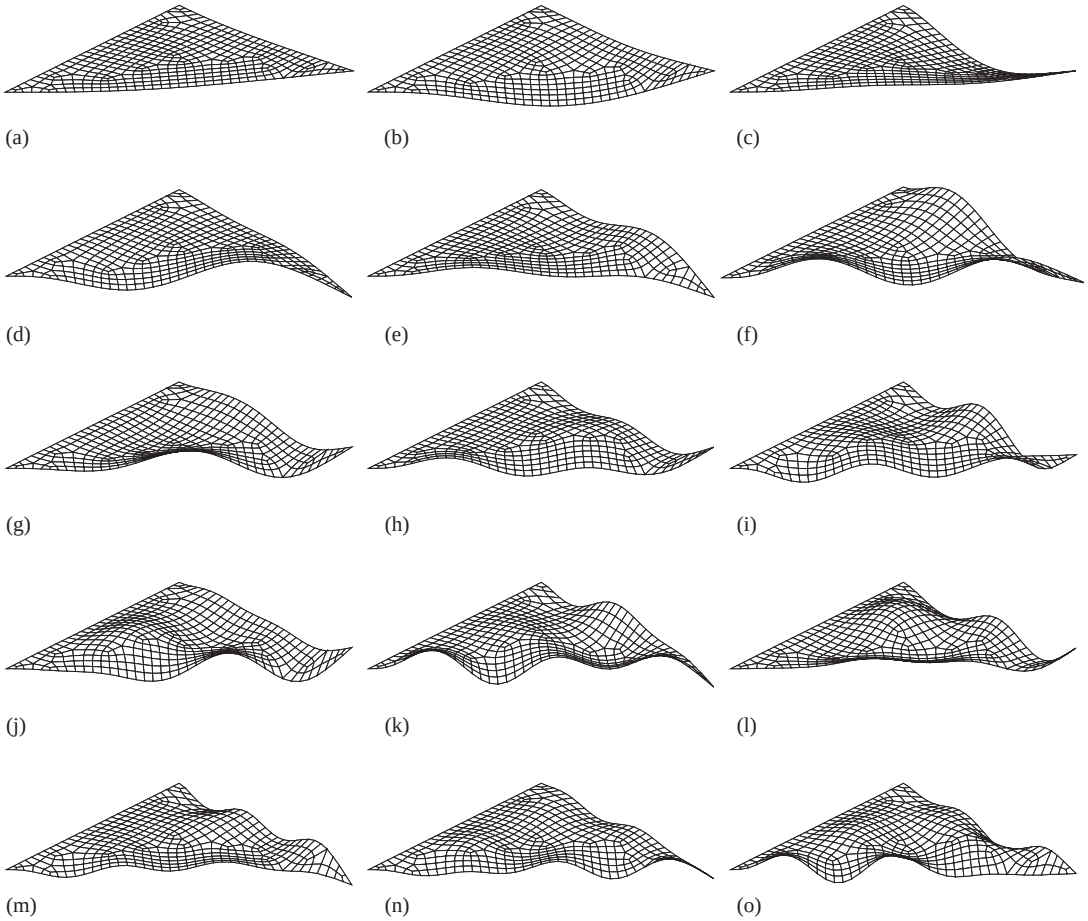

Fig. 12. Mode shapes of a triangular plate with the aspect ratio $h/a = 0.001$: (a) mode 1–(o) mode 15.

element based on the proposed formulation has performed well in most situations. It is shown that the present plate element is applicable to either thin or thick situations with enough accuracy.

Acknowledgements

The research grant from the Ministry of Science and Technology, Korea, for the Nuclear Research & Development Program is gratefully acknowledged.

References

[1] A.W. Leissa, Vibrations of plates, NASA SP-160, Washington, DC, 1969.
[2] A.W. Leissa, Recent research in plate vibrations: classical theory, *Shock Vibration Digest* 9 (1977) 13–24.

[3] A.W. Leissa, Plate vibration research: 1976–1980: classical theory, *Shock Vibration Digest* 13 (1981) 11–12.
[4] A.W. Leissa, Plate vibration research: 1981–1985: classical theory, *Shock Vibration Digest* 19 (1987) 11–18.
[5] K.M. Liew, Research on thick plate vibration: a literature survey, *Journal of Sound and Vibration* 180 (1995) 163–176.
[6] E. Reissner, The effect of transverse shear deformation on the bending of elastic plate, *American Society of Mechanical Engineers, Journal of Applied Mechanics* 12 (1945) 69–76.
[7] W.P. Doherty, E.J. Wilson, R.L. Taylor, Stress analysis of axisymmetric solids utilizing higher order quadrilateral finite element, UC-SESM Report No. 69–3, Department of Civil Engineering, University of California, Berkeley, 1969.
[8] O.C. Zienkiewicz, R.L. Taylor, J.M. Too, Reduced integration technique in general analysis of plates and shells, *International Journal for Numerical Methods in Engineering* 3 (1971) 275–290.
[9] K.J. Bathe, E.N. Dvorkin, A four-node plate bending element based on Mindlin–Reissner plate theory and a mixed formulation, *International Journal for Numerical Methods in Engineering* 21 (1985) 367–383.
[10] T. Belytschko, B.L. Wong, H. Stolarski, Assumed strain stabilization procedure for the 9-node Lagrangian shell element, *International Journal for Numerical Methods in Engineering* 28 (1989) 385–414.
[11] H.C. Huang, E. Hinton, A new nine node degenerated shell element with enhanced membrane and shear interpolation, *International Journal for Numerical Methods in Engineering* 22 (1986) 73–92.
[12] S.J. Lee, Y.B. Kim, Finite element analysis of laminated plates with assumed strain method, *Journal of the Architectural Institute of Korea* 10 (1994) 181–188.
[13] S.J. Lee, W. Kanok-Nukulchai, A nine-node assumed strain finite element for large-deformation analysis of laminated shells, *International Journal for Numerical Methods in Engineering* 4 (1998) 777–798.
[14] S.J. Lee, S.E. Han, Free-vibration analysis of plates and shells with a nine-node assumed natural degenerated shell element, *Journal of Sound and Vibration* 241 (2001) 605–633.
[15] K.J. Bathe, *The Finite Element Procedures in Engineering*, Prentice-Hall, Englewood Cliffs, NJ, 1987.
[16] E. Hinton, T.A. Rock, O.C. Zienkiwwicz, A note on mass lumping and related processes in finite element method, *International Journal for Numerical Methods in Engineering* 4 (1976) 245–249.
[17] T.J.R. Hughes, *The Finite Element Method—Linear Static and Dynamic Finite Element Analysis*, Prentice-Hall, Englewood Cliffs, NJ, 1987.
[18] B.S.Al. Janabi, E. Hinton, A study of the free vibrations of square plates with various edge conditions, in: E. Hinton (Ed.), *Numerical Methods and Software for Dynamic Analysis of Plates and Shells*, Pineridge Press, Swansea, 1988, pp. 167–204.
[19] D.J. Dawe, O.L. Roufaeil, Rayleigh–Ritz vibration analysis of Mindlin plates, *Journal of Sound and Vibration* 69 (1980) 345–359.
[20] A.W. Leissa, The free vibration of rectangular plates, *Journal of Sound and Vibration* 31 (1973) 257–293.
[21] E. Hinton, Dj. Vuksanovic, Closed form solutions for dynamic analysis of simply supported Mindlin plates, in: E. Hinton (Ed.), *Numerical Methods and Software for Dynamic Analysis of Plates and Shells*, Pineridge Press, Swansea, 1988, pp. 1–47.
[22] S. Srinivas, C.V. Joga Rao, A.K. Rao, An exact analysis for vibration of simply supported homogeneous and laminated, thick rectangular plates, *Journal of Sound and Vibration* 12 (1970) 187–199.
[23] J.N. Reddy, N.D. Phan, Stability and vibration of isotropic, orthotropic and laminated plates according to a higher-order shear deformation theory, *Journal of Sound and Vibration* 98 (1985) 157–170.
[24] D.J. Dawe, Finite strip models for vibration of Mindlin plates, *Journal of Sound and Vibration* 59 (1978) 441–452.
[25] P.S. Nair, S. Durvasula, Vibration of skew plates, *Journal of Sound and Vibration* 26 (1973) 1–19.
[26] T. Irie, G. Yamada, S. Aomura, Natural frequencies of Mindlin circular plates, *Journal of Applied Mechanics* 47 (1980) 652–655.
[27] K.Y. LAM, K.M. Liew, S.T. Chou, Use of two-dimensional orthogonal polynomials for vibration analysis of circular and elliptical plates, *Journal of Sound and Vibration* 154 (1992) 261–269.
[28] S. Mirza, M. Bijlani, Vibration of triangular plates, *American Institute of Aeronautics and Astronautics* 21 (1983) 1472–1475.

[29] P.N. Gustafson, W.F. Stokey, C.F. Zorowski, An experimental study of natural vibrations of cantilevered triangular plate, *Journal of Aeronautical Science* 20 (1953) 331–337.
[30] O.G. McGee, A.W. Leissa, C.S. Huang, Vibrations of cantilevered skewed trapezodial and triangular plates with corner stress singularities, *International Journal of Mechanical Science* 34 (1992) 63–84.
[31] W. Karunasena, S. Kitipornchai, F.G.A. Al-bermani, Free vibration of cantilevered arbitrary triangular mindlin plates, *International Journal of Mechanical Science* 38 (1996) 431–442.
[32] O.G. McGee, T.S. Butalia, Natural vibrations of shear deformable cantilevered skewed trapezodial and triangular thick plates, *Computers & Structures* 45 (1992) 1033–1059.